Oxidation and Reduction of Bis(imino)pyridine Iron Dinitrogen Complexes: Evidence for Formation of a Chelate Trianion.

Aaron M. Tondreau,[†] S. Chantal E. Stieber,[†] Carsten Milsmann,[†] Emil Lobkovsky,[‡] Thomas Weyhermüller,[§] Scott P. Semproni,[†] and Paul J. Chirik*,[†]

[†]Department of Chemistry, Princeton University, Princeton, New Jersey, 08544, United States

[‡]Department of Chemistry and Chemical Biology, Baker Laboratory, Cornell University, Ithaca, New York, 14853, United States

[§]Max-Planck Institute for Chemical Energy Conversion, Stiftstrasse 34-36, D-45470 Mülheim an der Ruhr, Germany

Ⓢ *Supporting Information*

ABSTRACT: Oxidation and reduction of the bis(imino)pyridine iron dinitrogen compound, (^{iPr}PDI)FeN$_2$ (^{iPr}PDI = 2,6-(2,6-^{i}Pr$_2$−C$_6$H$_3$−N=CMe)$_2$C$_5$H$_3$N) has been examined to determine whether the redox events are metal or ligand based. Treatment of (^{iPr}PDI)FeN$_2$ with [Cp$_2$Fe][BAr$^F_4$] (BAr$^F_4$ = B(3,5-(CF$_3$)$_2$-C$_6$H$_3$)$_4$) in diethyl ether solution resulted in N$_2$ loss and isolation of [(^{iPr}PDI)Fe(OEt$_2$)]-[BAr$^F_4$]. The electronic structure of the compound was studied by SQUID magnetometry, X-ray diffraction, EPR and zero-field ^{57}Fe Mössbauer spectroscopy. These data, supported by computational studies, established that the overall quartet ground state arises from a high spin iron(II) center (S_{Fe} = 2) antiferromagnetically coupled to a bis(imino)pyridine radical anion (S_{PDI} = 1/2). Thus, the oxidation event is principally ligand based. The one electron reduction product, [Na(15-crown-5)][(^{iPr}PDI)FeN$_2$], was isolated following addition of sodium naphthalenide to (^{iPr}PDI)FeN$_2$ in THF followed by treatment with the crown ether. Magnetic, spectroscopic, and computational studies established a doublet ground state with a principally iron-centered SOMO arising from an intermediate spin iron center and a rare example of trianionic bis(imino)pyridine chelate. Reduction of the iron dinitrogen complex where the imine methyl groups have been replaced by phenyl substituents, (^{iPr}BPDI)Fe(N$_2$)$_2$ resulted in isolation of both the mono- and dianionic iron dinitrogen compounds, [(^{iPr}BPDI)FeN$_2$]$^−$ and [(^{iPr}BPDI)FeN$_2$]$^{2-}$, highlighting the ability of this class of chelate to serve as an effective electron reservoir to support neutral ligand complexes over four redox states.
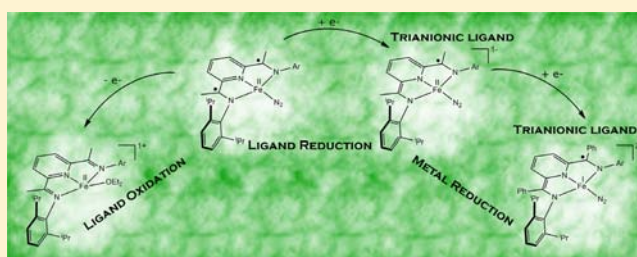
■ INTRODUCTION

Understanding the electronic structure of iron dinitrogen complexes is of fundamental and long-standing interest given the role of the base metal in industrial ammonia synthesis catalysts, its ubiquity in the active site in the nitrogenase family of enzymes, and recent demonstration of solution-phase N$_2$ hydrogenation and cleavage.[1,2] The emergence of bis(imino)pyridine iron dinitrogen compounds as precatalysts for olefin hydrogenation,[3−6] alkene[3,7] and ketone hydrosilylation,[8] intra-[9] and intermolecular[10] [2π + 2π] cycloaddition, and hydrogenative enyne and diyne cyclization[11] has prompted interest in determining the mechanism of action of this class of compounds. Before the fundamental steps that comprise catalytic cycles can be understood, the electronic structure of various types of iron dinitrogen compounds needs to be firmly established.

One notable feature of bis(imino)pyridines[12] is their ability to directly participate in the electronic structure of both coordination and organometallic compounds, acting either as redox noninnocent, π-acceptors or redox-active, radical-based ligands.[13−19] In iron chemistry, our laboratory has established the electronic structures of the four- and five-coordinate

dinitrogen compounds and related neutral ligand derivatives.[20−22] Spectroscopic and computational studies on the five-coordinate compound, (^{iPr}PDI)Fe(N$_2$)$_2$ (^{iPr}PDI = 2,6-(2,6-^{i}Pr$_2$−C$_6$H$_3$−N=CMe)$_2$C$_5$H$_3$N) established a highly covalent molecule best described as a hybrid between Fe(0) and Fe(II) oxidation states with resonance between the neutral and the closed-shell singlet dianionic form of the ligand (Figure 1). This electronic structure is similar to that established for the corresponding iron dicarbonyl, (^{iPr}PDI)Fe(CO)$_2$.[20,23]

Dissociation of one of the N$_2$ ligands yields (^{iPr}PDI)FeN$_2$, a compound with a distinct electronic structure from (^{iPr}PDI)Fe(N$_2$)$_2$.[21] This molecule is best described as an intermediate spin ferrous compound antiferromagnetically coupled to a bis(imino)pyridine triplet diradical dianion. A low-lying paramagnetic excited state is thermally accessible at ambient temperature and gives rise to dispersed ^{1}H NMR chemical shifts.[21,24] Related four-coordinate compounds with principally σ-donating ligands such as (^{iPr}PDI)Fe(DMAP) (DMAP = 4-N,N-(dimethylamino)pyridine) and (^{iPr}PDI)FeNH$_3$[25] are also
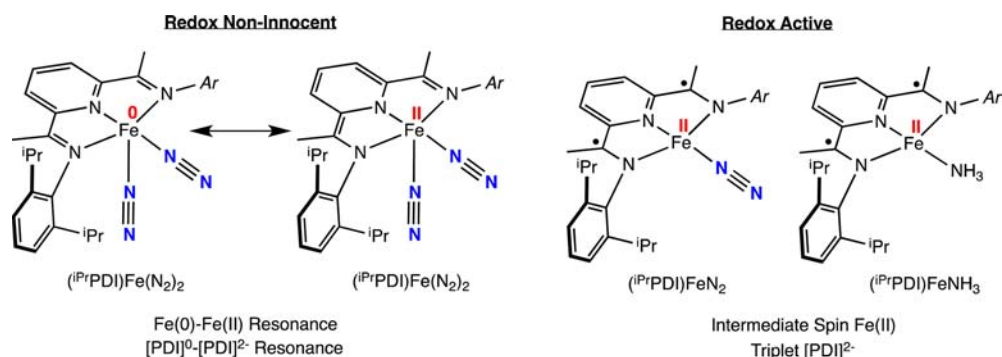
Figure 1. Electronic structures of $(^{iPr}PDI)Fe(N_2)_2$, $(^{iPr}PDI)FeN_2$ and $(^{iPr}PDI)FeNH_3$.
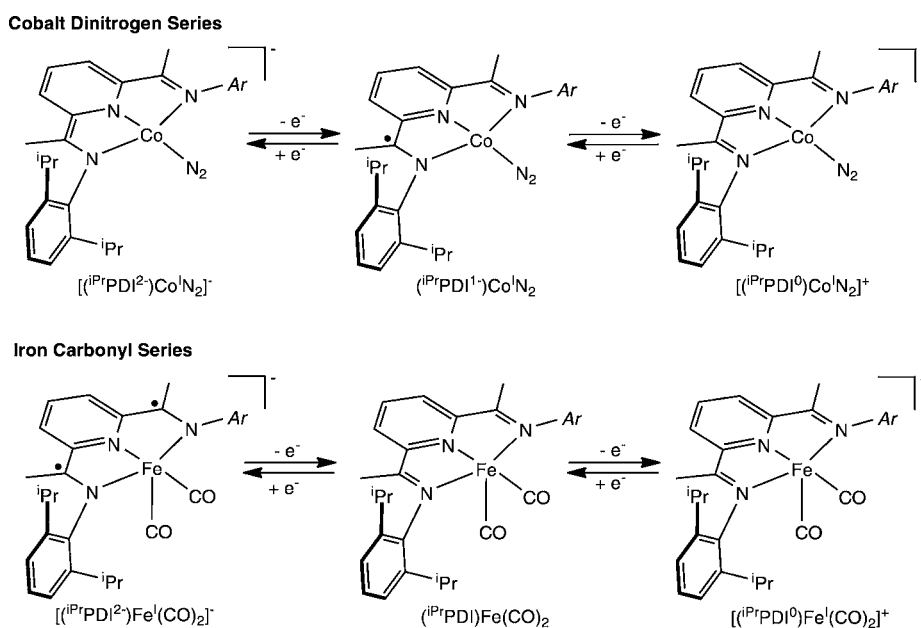
Figure 2. Electronic structures of redox series of bis(imino)pyridine cobalt dinitrogen compounds and iron carbonyl derivatives.

intermediate spin ferrous compounds antiferromagnetically coupled to bis(imino)pyridine triplet diradical dianions. However, mixing of the paramagnetic excited state into the ground state by spin−orbit coupling gives rise to temperature independent paramagnetism and different NMR spectroscopic properties than $(^{iPr}PDI)FeN_2$.

Gambarotta and co-workers have independently reported additional synthetic studies on the reduction of $(^{iPr}PDI)FeCl_2$ with various amounts of NaH in the presence of N_2. This work has expanded the number of known structural types in this family of iron dinitrogen compounds.[26] Addition of three equivalents of NaH yielded an anionic iron dinitrogen compound where the bis(imino)pyridine has been deprotonated and the sodium is coordinated side-on to the terminal N_2 ligand. Increasing the number of equivalents of NaH used resulted in isolation and structural characterization of different anionic dinitrogen complexes with varying Na solvation and degrees of bis(imino)pyridine modification.

The establishment of the electronic structures of the neutral four- and five-coordinate bis(imino)pyridine iron dinitrogen complexes, $(^{iPr}PDI)Fe(N_2)_2$ and $(^{iPr}PDI)FeN_2$, raised interest in the oxidation and reduction of these compounds. In addition to the fundamental question as to whether the redox events are metal or ligand based, synthetic efforts of this type may also yield new catalyst precursors. Recently our laboratory reported

the synthesis and characterization of a series of bis(imino)-pyridine cobalt dinitrogen complexes[27] and a family of bis(imino)pyridine iron dicarbonyl complexes that differ by three oxidation states (Figure 2).[23]

In the iron series, the presence of weaker field N_2 ligands may give rise, as in the neutral cases, to electronic structures distinct from the iron dicarbonyl family of compounds. Outside the realm of bis(imino)pyridine compounds, Peters and co-workers have reported a series of trigonal bipyramidal iron dinitrogen derivatives in three formal oxidation states (0, I, and II) and explored N_2 functionalization chemistry from these platforms.[28] Here we describe the oxidation and reduction of $(^{iPr}PDI)FeN_2$ and the reduction of the phenyl-substituted analog, $(^{iPr}BPDI)Fe(N_2)_2$ ($^{iPr}BPDI = 2,6-(2,6-^{i}Pr_2−C_6H_3−N=CPh)_2C_5H_3N$). The electronic structures of all of the compounds in this study were elucidated using a combination of spectroscopic, X-ray diffraction and computational techniques, and a rare example of a trianionic bis(imino)pyridine ligand has been identified.

■ RESULTS AND DISCUSSION

Oxidation and Reduction of Bis(imino)pyridine Iron Dinitrogen Compounds. Our studies commenced with the oxidation of the neutral bis(imino)pyridine iron dinitrogen

complex, $(^{iPr}PDI)FeN_2$. Treatment of a diethyl ether solution of $(^{iPr}PDI)FeN_2$ with $[Cp_2Fe][BAr^F_4]$ resulted in gas evolution and formation of a light green solution from which $[(^{iPr}PDI)Fe(OEt_2)][BAr^F_4]$ was isolated as light green powder in 73% yield following recrystallization at $-35\ ^\circ C$ (eq 1). Note that the

$$(1)$$
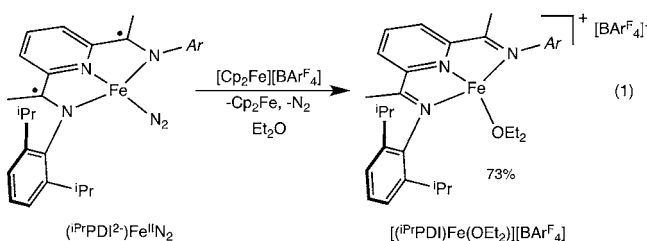
iron compounds are depicted in their traditional form until the data have been presented to establish the electronic structure of the molecule and role of the bis(imino)pyridine ligand.

The solid-state structure of $[(^{iPr}PDI)Fe(OEt_2)][BAr^F_4]$ was determined by single-crystal X-ray diffraction and a representation of the cationic iron portion of the molecule is presented in Figure 3. Selected bond distances and angles are reported in
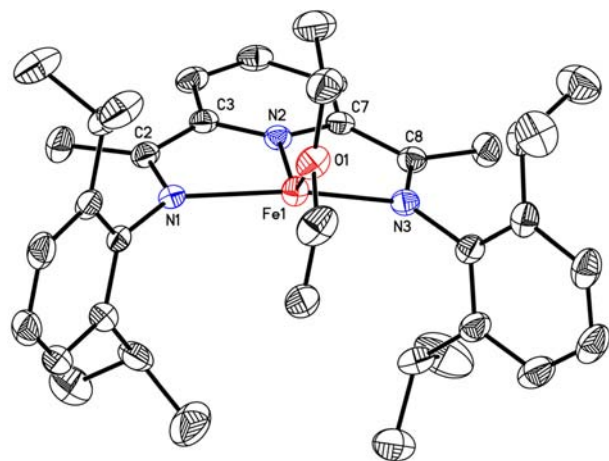

Figure 3. Molecular structure of the cation of $[(^{iPr}PDI)Fe(OEt_2)]$-$[BAr^F_4]$ at 30% probability ellipsoids. Anion and hydrogen atoms omitted for clarity. A depiction of the full molecule is presented in the Supporting Information.

Table 1. Selected Bond Distances (Å) and Angles (deg) for $[(^{iPr}PDI)Fe(OEt_2)][BAr^F_4]$

Fe(1)−N(1)	2.109(2)
Fe(1)−N(2)	1.954(2)
Fe(1)−N(3)	2.106(3)
Fe(1)−O(1)	2.015(2)
N(1)−C(2)	1.301(4)
N(3)−C(8)	1.301(4)
N(2)−C(3)	1.349(4)
N(2)−C(7)	1.357(4)
C(2)−C(3)	1.441(4)
C(7)−C(8)	1.448(4)
N(1)−Fe(1)−N(2)	76.89(10)
N(1)−Fe(1)−N(3)	145.53(10)
N(2)−Fe(1)−N(3)	77.39(10)
N(2)−Fe(1)−O(1)	138.12(10)

Table 1. The crystallographic data establish formation of the bis(imino)pyridine iron diethyl ether cation where the oxygen atom is lifted by 41° out of the metal-chelate plane. There are no close contacts between the cation and anion, suggesting that such interactions are not the cause of the distortion from planarity. Infrared spectroscopy on the bulk material revealed no strong bands assignable to N_2 stretches, consistent with the crystal being representative of the bulk product. The distortions to the chelate are modest yet are more consistent with a one electron reduced rather than neutral bis(imino)pyridine as evidenced by the $N_{imine}-C_{imine}$ distances of 1.301(4) and 1.301(4) Å and the $C_{imine}-C_{ipso}$ bond lengths of 1.441(4) and 1.448(4) Å. The $Fe-N_{imine}$ distances of 2.109(2) and 2.106(3) are elongated and are diagnostic for a high spin iron compound, consistent with the magnetic data (vide infra). The observation of a bis(imino)pyridine radical anion and paramagnetic, high spin iron center are consistent with an $S_{Fe} = 2$ ferrous compound.

To further elucidate the electronic structure of $[(^{iPr}PDI)Fe(OEt_2)][BAr^F_4]$, the compound was studied by zero-field ^{57}Fe Mössbauer spectroscopy. The spectrum recorded in the solid state at 80 K exhibits a quadrupole doublet (Figure 4) with an
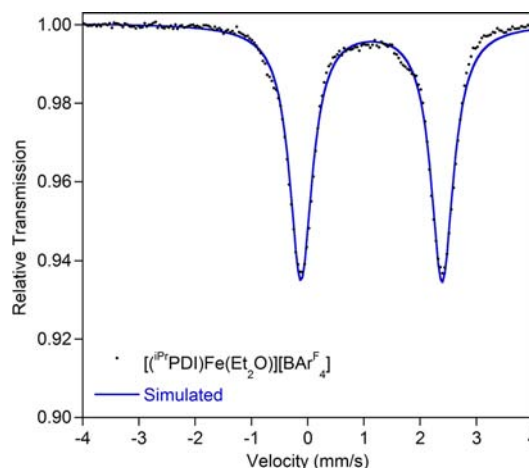

Figure 4. Zero-field ^{57}Fe Mössbauer spectrum of $[(^{iPr}PDI)Fe(OEt_2)]$-$[BAr^F_4]$ at 80 K.

isomer shift of 1.13 mm/s and $\Delta E_Q = 2.51$ mm/s, consistent with a high spin iron(II) compound. The isomer shift is one of the highest observed in bis(imino)pyridine iron chemistry and highlights the weak ligand field imparted by the monoreduced form of the chelate and the diethyl ether ligand.

The magnetic properties of $[(^{iPr}PDI)Fe(OEt_2)][BAr^F_4]$ were studied by variable temperature solid-state SQUID magnetometry (see the Supporting Information). At temperatures above 40 K, the data plateau at 4.4 μB, slightly higher than the spin only value for three unpaired electrons, consistent with an $S = 3/2$ ground state and a high spin Fe(II) center antiferromagnetically coupled to a monoreduced bis(imino)pyridine radical.

The benzene-d_6 ^1H NMR spectrum of $[(^{iPr}PDI)Fe(OEt_2)]$-$[BAr^F_4]$ exhibited peaks only for the anion; no resonances assignable to the bis(imino)pyridine iron cation were observed. The ^{19}F NMR spectrum exhibited a single sharp peak centered at 62.30 ppm suggesting little interaction of $[BAr^F_4]^-$ with the paramagnetic iron center in solution. The lack of observable NMR resonances prompted further investigation by EPR spectroscopy. Attempts to record the spectrum in a toluene

glass at 77 K did not yield reliable data due to precipitation of the iron compound. Use of a diethyl ether glass obviated these complications. A representative EPR spectrum recorded at 77 K along with the simulation of the data are presented in Figure 5.
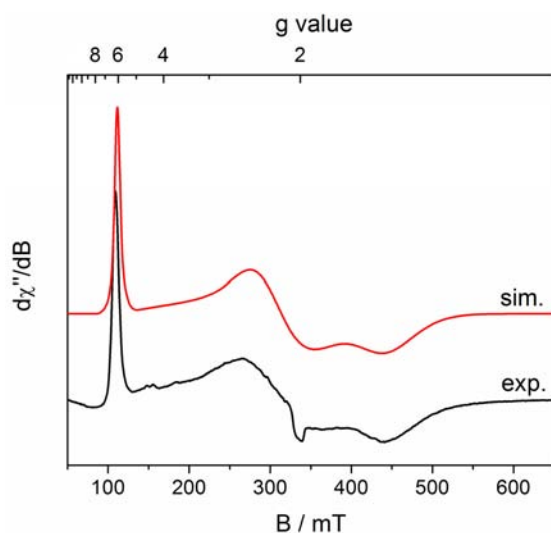

Figure 5. X-band EPR spectrum of $[(^{iPr}PDI)Fe(OEt_2)][BAr^F_4]$ recorded at 77 K in diethyl ether glass (black). Simulated spectrum (red): $g_x = 2.11$, $g_y = 2.22$, $g_z = 2.03$ ($g_{avg} = 2.12$), $D = 9.6$ cm^{-1} and $E/D = 0.33$.

A rhombic signal, consistent with an $S = 3/2$ complex, was observed. The spectrum was successfully simulated using an $S = 3/2$ spin Hamiltonian formalism using the large ZFS parameter $D = 9.6$ cm^{-1} ($D \gg h\nu \approx 0.3$ cm^{-1} at X-band) consistent with the magnetic susceptibility measurements, full rhombicity $E/D = 0.33$ and $g_x = 2.11$, $g_y = 2.22$, $g_z = 2.03$ ($g_{avg} = 2.12$). A distribution of the rhombicity (E/D-strain, $\sigma(E/D) = 0.035$) was imposed to model the line broadening resulting from microheterogeneities in the sample. The anisotropic g values support a majority contribution of metal-centered spin density to the total spin of the molecule which is in good agreement with the electronic structure description as a high-spin Fe(II) center antiferromagnetically coupled to a bis(imino)pyridine radical anion. The analogous cobalt complex, $[(^{iPr}PDI)Co-(OEt_2)]^+$, was previously reported[29] and is a diamagnetic molecule resulting from antiferromagnetic coupling of a low spin Co(II) center to a bis(imino)pyridine anion.

The successful oxidation of $(^{iPr}PDI)FeN_2$ prompted studies into the corresponding reduction chemistry. In principle, cyclic voltammetry would provide insight into both oxidative and reductive events associated with $(^{iPr}PDI)FeN_2$. However, dissolving $(^{iPr}PDI)FeN_2$ in THF, a common solvent for such measurements, results in immediate N$_2$ dissociation and formation of $(^{iPr}PDI)Fe(THF)_n$.[3,4] Accordingly, chemical methods were explored exclusively. As with $(^{iPr}PDI)Fe(CO)_2$,[23] the reduction of $(^{iPr}PDI)FeN_2$ proved more challenging than the corresponding oxidation. Treatment of a THF solution of $(^{iPr}PDI)FeN_2$ with 1.05 equiv of sodium naphthalenide followed by solvent removal and washing with diethyl ether furnished a dark red brown solid identified as $[Na(THF)_n]-[(^{iPr}PDI)Fe(N_2)]$. Analysis of the product mixture by solid-state (KBr) infrared spectroscopy revealed two bands, centered at 1966 and 1917 cm^{-1}. All infrared stretching frequencies for the anionic iron dinitrogen compounds prepared in this work

are reported in Table 2. For $[Na(THF)_n][(^{iPr}PDI)Fe(N_2)]$, the two bands likely arise from two different compounds with

Table 2. Solid-State (KBr) Infrared Stretching Frequencies (in cm^{-1}) of Various Bis(imino)pyridine Iron Dinitrogen Anions

compd	$\nu(N_2)$ (cm^{-1})
$(^{iPr}PDI)Fe(N_2)^a$	2036
$[Na(THF)_n][(^{iPr}PDI)Fe(N_2)]$	1966, 1917
$[Na(15\text{-}crown\text{-}5)(THF)_2][(^{iPr}PDI)Fe(N_2)]$	1956
$[Na(18\text{-}crown\text{-}6)(THF)_2][(^{iPr}PDI)Fe(N_2)]$	1949
$[Na(THF)_n][(^{iPr}BPDI)Fe(N_2)]$	1979, 1932
$[Na(18\text{-}crown\text{-}6)(THF)_2][(^{iPr}BPDI)Fe(N_2)]$	1971
$[Na(THF)_n]_2[(^{iPr}BPDI)Fe(N_2)]$	1908, 1830
$[Na(18\text{-}crown\text{-}6)(THF)_2]_2[(^{iPr}BPDI)Fe(N_2)]$	1887

^{a}Data taken from ref 3.

different sodium coordination modes, similar to observations reported by Gambarotta and co-workers.[26] To confirm that the bis(imino)pyridine ligand was intact and did not undergo deprotonation,[30−33] we treated the mixture of bis(imino)-pyridine iron dinitrogen anions, in separate experiments, with either Me$_3$SiCl or $[Cp_2Fe][BPh_4]$. In both cases, $(^{iPr}PDI)FeN_2$ was obtained as the sole iron compound, suggesting that the bis(imino)pyridine chelate was not modified during the reduction.

Because of the complications of variable sodium coordination environments, characterization of the mixture of $[Na(THF)_n]-[(^{iPr}PDI)Fe(N_2)]$ compounds was not undertaken. Even if these compounds were fully characterized, interaction of the sodium cation with different portions of the bis(imino)pyridine ligand would render interpretation of redox-activity of the chelate ambiguous. To obviate these complications, two different strategies were pursued. The first involved reduction of $(^{iPr}PDI)FeN_2$ with magnesium activated with either anthracene or isoprene. Both activation methods resulted in rapid reduction of $(^{iPr}PDI)FeN_2$; however, multiple N$_2$ stretches were observed by infrared spectroscopy, diagnostic of various interactions with the bis(imino)pyridine and dinitrogen ligands.

Because changing the nature of the reductant did not result in an anionic iron dinitrogen complex devoid of interactions with the cation, methods for the encapsulation of the sodium were pursued. The anionic iron dinitrogen compound, $[Na(THF)_n][(^{iPr}PDI)Fe(N_2)]$, was generated in THF solution, filtered through Celite and then treated with either 15-crown-5 or 18-crown-6 to yield $[Na(15\text{-}crown\text{-}5)(THF)_2][(^{iPr}PDI)Fe-(N_2)]$ and $[Na(18\text{-}crown\text{-}6)(THF)_2][(^{iPr}PDI)Fe(N_2)]$, respectively, as dark brown solids (eq 2).
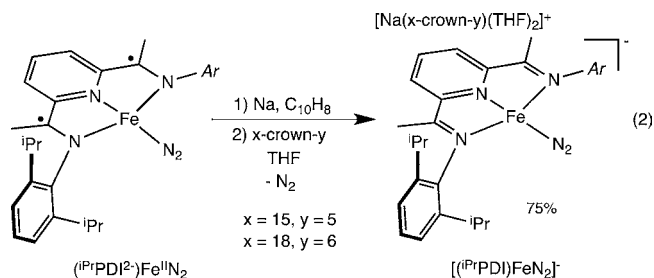
The syntheses of $[Na(15\text{-}crown\text{-}5)(THF)_2][(^{iPr}PDI)Fe-(N_2)]$ and $[Na(18\text{-}crown\text{-}6)(THF)_2][(^{iPr}PDI)Fe(N_2)]$ in the

presence of excess THF are notable when compared to the corresponding neutral and cationic compounds. Oxidation of $(^{iPr}PDI)Fe(N_2)_2$ in diethyl ether resulted in immediate dinitrogen dissociation to form the corresponding iron diethyl ether complex. The neutral bis(imino)pyridine iron compound also undergoes rapid substitution of coordinated N_2 upon dissolution in THF to form $(^{iPr}PDI)Fe(THF)_2$ (see the Supporting Information).[3,4] The anionic iron dinitrogen compounds are prepared in THF and show no evidence for N_2 displacement following reduction. The reduced compounds have a preference for coordination of π-acids, likely a consequence of the electronic structure of the anions. Both compounds exhibit single strong N≡N bands centered at 1956 (15-crown-5) and 1949 (18-crown-6) cm^{-1} in the solid state. These values are reduced from the stretching frequency of 2036 cm^{-1} reported for the neutral four-coordinate iron dinitrogen complex, $(^{iPr}PDI)FeN_2$.[3,21] The solid-state magnetic susceptibility of both anionic iron dinitrogen compounds were measured using a magnetic susceptibility balance at 23 °C and values of 1.9 μB (15-crown-5) and 1.8 μB (18-crown-6) were obtained and are consistent with $S = 1/2$ compounds.

The solid-state structure of $[Na(15\text{-crown-}5)(THF)_2]$-$[(^{iPr}PDI)Fe(N_2)]$ was determined by X-ray diffraction and a representation of the anionic portion of the molecule is presented in Figure 6. A depiction of the full molecule is
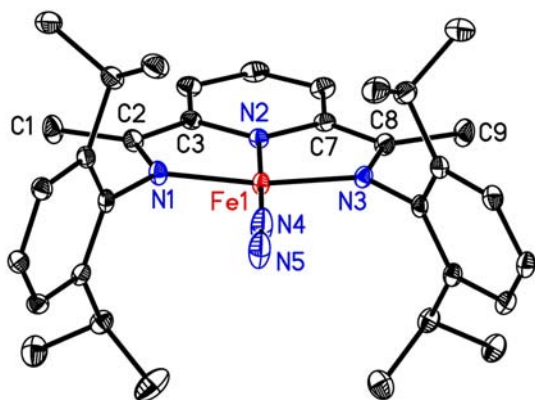

Figure 6. Molecular structure of the iron anion of $[Na(15\text{-crown-}5)(THF)_2][(^{iPr}PDI)Fe(N_2)]$ at 30% probability ellipsoids. Cation and hydrogen atoms omitted for clarity. A depiction of the full molecule is presented in the Supporting Information.

presented in the Supporting Information. A lower-quality, disordered structure was also obtained for $[Na(18\text{-crown-}6)(THF)_2][(^{iPr}PDI)Fe(N_2)]$ and is reported in the Supporting Information. For the 15-crown-5 derivative, the cation does not exhibit any close contacts to the iron anion. The geometry of the iron anion is best described as idealized planar, similar to neutral four-coordinate mono(dinitrogen) compounds.[21] The metrical parameters of the bis(imino)pyridine (Table 3) signal significant chelate distortions as the $C_{imine}-C_{ipso}$ distances are contracted to 1.405(3) and 1.400(3) Å and the $N_{imine}-C_{imine}$ distances are expanded to 1.391(3) and 1.389(3) Å. These distortions are some of the most pronounced observed in an bis(imino)pyridine iron compound and surpass the range typically ascribed to two electron ligand reduction.[3,14]

The electronic structure of $[Na(15\text{-crown-}5)(THF)_2]$-$[(^{iPr}PDI)Fe(N_2)]$ was also studied by zero-field Mössbauer spectroscopy at 80 K. The experimentally determined parameters for this and all of the iron complexes examined in

Table 3. Selected Bond Distances (Å) and Angles (deg) for $[Na(15\text{-crown-}5)(THF)_2] [(^{iPr}PDI)Fe(N_2)]$

Fe(1)−N(1)	1.8858(18)
Fe(1)−N(2)	1.8338(17)
Fe(1)−N(3)	1.8912(18)
Fe(1)−N(4)	1.784(2)
N(1)−C(2)	1.366(3)
N(3)−C(8)	1.375(3)
N(2)−C(3)	1.391(3)
N(2)−C(7)	1.389(3)
C(2)−C(3)	1.405(3)
C(7)−C(8)	1.400(3)
N(4)−N(5)	1.089(3)
N(1)−Fe(1)−N(2)	80.82(8)
N(1)−Fe(1)−N(3)	161.68(7)
N(2)−Fe(1)−N(3)	80.91(8)
N(2)−Fe(1)−N(4)	161.68(7)

this study are reported in Table 4. The experimentally determined isomer shift (δ) of 0.28 mm/s is lower than the

Table 4. Zero-Field ^{57}Fe Mössbauer Spectral Parameters for Various Anionic Bis(imino)pyridine Iron Dinitrogen Compounds and Cationic Diethyl Ether Complex, $[(^{iPr}PDI)Fe(OEt_2)_n]^+$; Data for Neutral $(^{iPr}PDI)Fe(N_2)_2$, $(^{iPr}PDI)Fe(N_2)$, and $(^{iPr}BPDI)Fe(N_2)_2$ are Included for Comparison[6,22a]

compd	δ (mm/s)	ΔE_Q (mm/s)
$[(^{iPr}PDI)Fe(OEt_2)]^+$	1.13	2.51
$(^{iPr}PDI)Fe(N_2)_2$	0.39	−0.53
$(^{iPr}PDI)FeN_2$	0.38	+1.72
$[(^{iPr}PDI)Fe(N_2)]^-$	0.28	1.66
$(^{iPr}BPDI)Fe(N_2)_2$	0.43	1.91
$[(^{iPr}BPDI)Fe(N_2)]^-$	0.30	1.93
$[(^{iPr}BPDI)Fe(N_2)]^{2-}$	0.15	1.49

^{a}All spectra were recorded at 80 K.

values of 0.38 and 0.39 mm/s previously reported for the four- and five-coordinate neutral compounds, $(^{iPr}PDI)FeN_2$ and $(^{iPr}PDI)Fe(N_2)_2$, indicating a higher degree of covalency resulting from a more π-acidic bis(imino)pyridine.

The X-band EPR spectrum of $[Na(15\text{-crown-}5)(THF)_2]$-$[(^{iPr}PDI)Fe(N_2)]$ was recorded in toluene glass at 77 K and the experimental data along with the simulation are presented in Figure 7. A rhombic signal is observed that is consistent with an $S = 1/2$ system. The data were simulated using a spin Hamiltonian and g-values of 1.95, 2.15 and 2.24, $g_{avg} = 2.11$. The large g anisotropy and the strong deviation of the g_{avg} value from the free-electron $g = 2$ support a system with metal-centered spin. The signal at $g = 2$ is due to a small amount of organic radical impurity.

On the basis of the precedent established by Gambarotta,[26] we were unsure if deprotonation of the imine methyl groups in the bis(imino)pyridine chelate would complicate the reduction reactions.[31] Parallel studies were therefore conducted with the iron dinitrogen complex where the imine methyl groups were replaced by phenyl substituents, $(^{iPr}BPDI)Fe(N_2)_2$ ($^{iPr}BPDI = 2,6\text{-}(2,6\text{-}^iPr_2\text{-}C_6H_3N═CPh)_2C_5H_3N)$). Previous studies have also shown that this chelate is electron deficient compared to the methylated variant and may more readily accept electron density.[4,34]
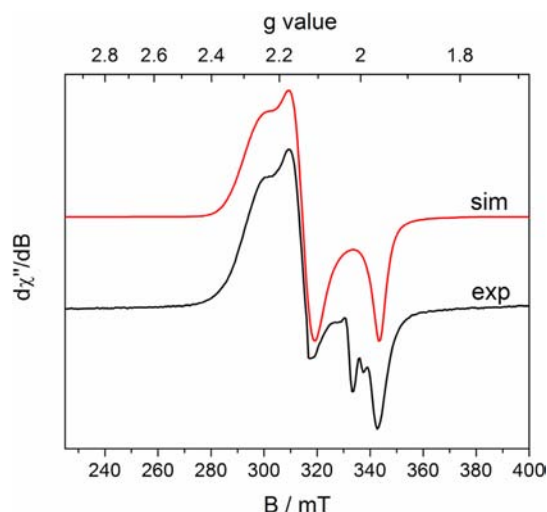
639

dx.doi.org/10.1021/ic301675t | Inorg. Chem. 2013, 52, 635–646

Figure 7. X-band EPR spectrum of $[Na(15\text{-crown-}5)(THF)_2]$-$[(^{iPr}PDI)Fe(N_2)]$ recorded in toluene glass at 77 K (black). Simulated spectrum (red) with g values =1.95, 2.15, and 2.24 and a $g_{average}$ = 2.11.

Figure 8. X-band EPR spectrum of $[Na(15\text{-crown-}5)(THF)_2]$-$[(^{iPr}BPDI)Fe(N_2)]$ recorded in toluene glass at 77 K (black). Simulated spectrum (red) g-values of 1.97, 2.13, and 2.24, $g_{average}$ = 2.11.

Addition of $(^{iPr}BPDI)Fe(N_2)_2$ to a THF solution containing 1.05 equivalents of sodium naphthalenide resulted in a color change from red to pink. Removing the volatiles in vacuo followed by extraction into diethyl ether and recrystallization from pentane at −35 °C resulted in isolation of pink-red crystals identified as $[Na(THF)_n][(^{iPr}BPDI)Fe(N_2)]$. Similar to the methylated compound, analysis of the crystals by solid-state infrared spectroscopy produced two N≡N bands at 1979 and 1932 cm^{-1}, likely due to different interactions of the iron compound with the sodium cation. These values are at slightly higher frequency than for the methylated iron dinitrogen anion, $[(^{iPr}PDI)Fe(N_2)]^-$, as expected for the more electron withdrawing $[^{iPr}BPDI]$ chelate.[3,4]

Encapsulation of the sodium cation was accomplished by treating the THF derivative with 18-crown-6 and yielded a bright pink solid identified as $[Na(18\text{-crown-}6)(THF)_2]$-$[(^{iPr}BPDI)Fe(N_2)]$ in 73% yield. As with the methylated compound, $[Na(18\text{-crown-}6)(THF)_2][(^{iPr}BPDI)Fe(N_2)]$ exhibits a solid state magnetic moment of 1.7 μB, consistent with an $S = 1/2$ ground state. The solid state infrared stretching frequency of 1971 cm^{-1} is more reduced than the neutral dinitrogen compound but at a higher frequency than the corresponding anion with the methylated backbone. An EPR spectrum was recorded at 77 K in frozen toluene glass and is presented in Figure 8. The data were simulated for an $S = 1/2$ system using a spin Hamiltonian with g-values of 1.97, 2.13, and 2.24. The g-values and g_{avg} = 2.11 are similar to those of the methylated variant, suggesting metal-centered spins and similar electronic environments for both compounds.

Perhaps somewhat surprisingly, $[(^{iPr}BPDI)Fe(N_2)]^-$ could be reduced by an additional electron. Stirring a THF solution of the neutral dinitrogen complex, $(^{iPr}BPDI)Fe(N_2)_2$, with three equivalents of sodium metal in the presence of a catalytic amount of naphthalene furnished the bis(imino)pyridine iron dinitrogen dianion, $[Na(THF)_n]_2[(^{iPr}BPDI)Fe(N_2)]$. Strong N_2 stretches centered at 1908 and 1830 cm^{-1} were observed in the solid-state infrared spectrum and proved valuable for routine characterization of bulk samples. Although isolated samples are diamagnetic as judged by magnetic susceptibility balance, NMR spectroscopy proved uninformative as only THF resonances were observed in THF-d_8 solution. Because of the
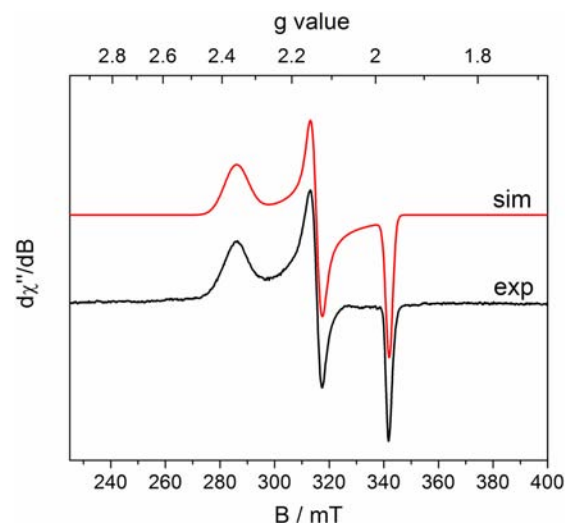
extreme sensitivity and poor solubility of the compound, reliable solution magnetic moments could not be obtained.

Single crystals of $[Na(THF)_2][Na(OEt_2)_2][(^{iPr}BPDI)Fe(N_2)]$ were obtained from a diethyl ether-THF solution at −35 °C. A representation of the molecule is presented in Figure 9 and metrical data are reported in the Supporting
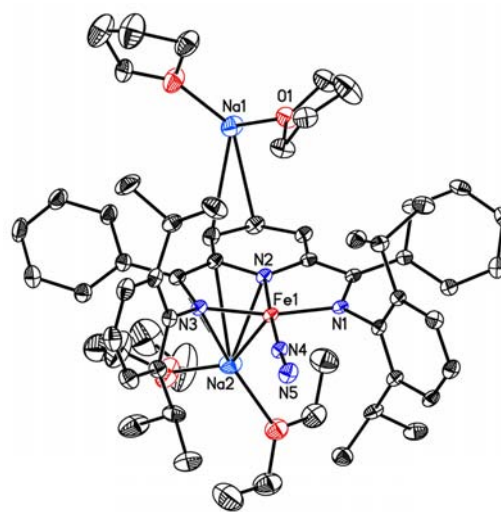

Figure 9. Solid-state structure of $[Na(THF)_2][Na(OEt_2)(THF)]$-$[(^{iPr}BPDI)Fe(N_2)]$ at 30% probability ellispoids. Hydrogen atoms omitted for clarity.

Information. We note that the crystals are extremely sensitive and challenging to handle and isolate in reasonable quantities. The structural data establish a pseudo four-coordinate, idealized planar bis(imino)pyridine iron dinitrogen compound with one of the sodium cations coordinated to the C(11)−C(12) positions of the pyridine with two molecules of THF completing the coordination sphere. The second sodium cation interacts with one of the pyridine imine portions of the chelate and is solvated by one THF and one diethyl ether molecule. Incorporation of the diethyl ether ligands is likely a

consequence of the recrystallization conditions. This structure, along with the previously reported structures of Gambarotta,[26] confirms the variable coordination modes for sodium cations with bis(imino)pyridine anions and further highlights the value in encapsulation with crown ethers. The N(4)−N(5) distance of 1.148(2) Å is consistent with little reduction by the iron center.

As with other compounds reported in this work, encapsulation of the sodium cations was accomplished by treating the THF solution of the initially formed dianion with 18-crown-6 to furnish a diamagnetic, purple solid identified as $[Na(18\text{-crown-}6)(THF)_2]_2[(^{iPr}BPDI)Fe(N_2)]$ in 70% yield. $[Na(18\text{-crown-}6)(THF)_2]_2[(^{iPr}BPDI)Fe(N_2)]$ produced a single strong band centered at 1887 cm^{-1} and as expected, is the most reduced dinitrogen ligand in the series. The zero-field ^{57}Fe Mössbauer spectrum was recorded at 80 K and exhibits an isomer shift of 0.15 mm/sec and a quadrupole splitting of 1.49 mm/s.

Computational Studies. The oxidation and reduction products of the bis(imino)pyridine iron dinitrogen compounds were studied by broken symmetry DFT calculations to gain additional insight into the electronic structure of the compounds. In the broken symmetry notation, BS(m, n) describes a state in which there are m unpaired spin-up electrons and n unpaired spin-down electrons on separate fragments.[35−37] Our studies commenced with computations on the cationic iron diethyl ether complex, $[(^{iPr}PDI)Fe(OEt_2)]^+$ at the B3LYP level of DFT. Although the anion was omitted from the calculation, no additional truncations were made. The computed ground state obtained using a simple unrestricted quartet approach corresponds to a broken symmetry (4,1) solution and successfully reproduces the deviation of the diethyl ether ligand from iron-chelate plane. The computed Mössbauer parameters of δ = 1.00 mm/s and ΔE_Q = 2.75 mm/s are in acceptable agreement with the experimentally determined values of δ = 1.13 mm/s and ΔE_Q = 2.51 mm/s. A qualitative molecular orbital diagram and the computed spin density from the BS(4,1) solution are presented in Figure 10 and are consistent with a high spin iron(II) center (S_{Fe} = 2) antiferromagnetically coupled to a bis(imino)pyridine radical anion. The deviation of the diethyl ether ligand from planarity is likely a result of the high spin state and population of the $d_{x^2-y^2}$-based molecular orbital. Notably, the computational studies are fully consistent with the experimental data and firmly establish the electronic structure of the bis(imino)-pyridine iron cation.

The computational results of the bis(imino)pyridine iron dinitrogen monoanion were less straightforward. Using the coordinates from the higher quality X-ray crystal structure, $[Na(15\text{-crown-}5)(THF)_2][(^{iPr}PDI)Fe(N_2)]$ as the starting point, spontaneous symmetry breaking in an unrestricted doublet calculation resulted in an unusual BS(1,2) solution corresponding to a low-spin Fe(I) center (S_{Fe} = 1/2) with a triplet bis(imino)pyridine radical dianion (S_{PDI} = 1). Antiferromagnetic coupling (S = 0.40) between the metal d_{yz} and ^{iPr}PDI a_2 molecular orbitals accounts for the overall doublet ground state. In this description, the SOMO of the compound is essentially ligand based with dominant b_2 PDI character. If this electronic structure description was indeed correct, the one electron reduction of $(^{iPr}PDI^{2-})Fe^{II}N_2$ would be iron-based, preserving the triplet diradical bis(imino)pyridine dianion.

Comparisons of selected computed and experimental selected metrical and Mössbauer parameters are presented in
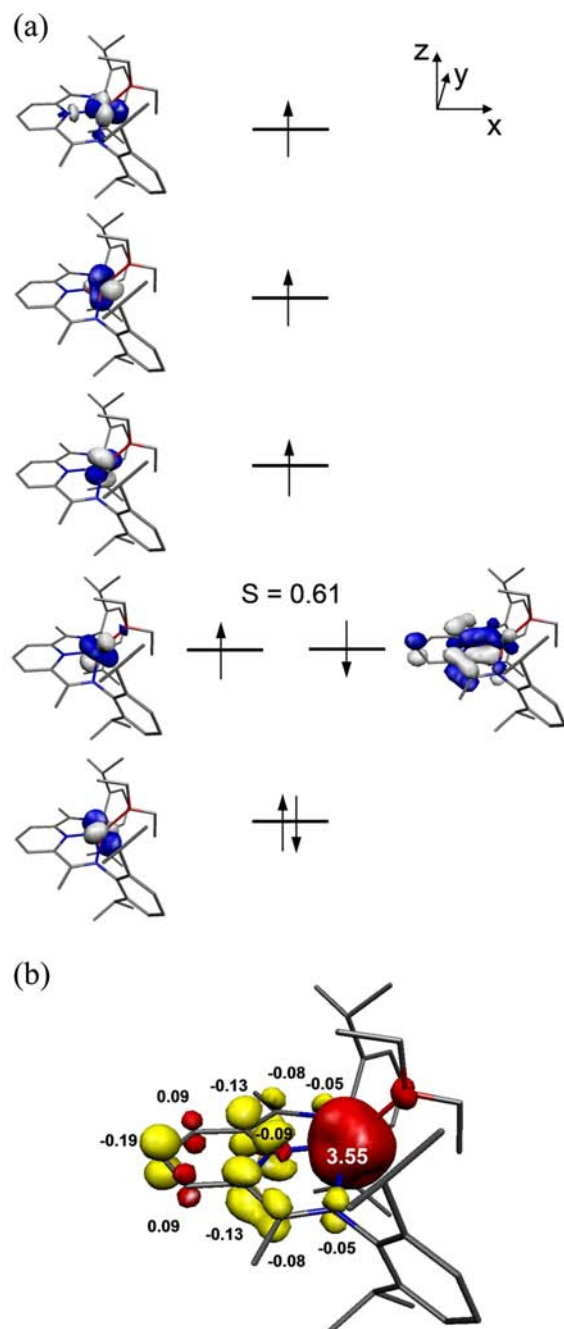

Figure 10. (a) Qualitative molecular orbital diagram for $[(^{iPr}PDI)Fe(OEt_2)]^+$ from a spin-unrestricted B3LYP DFT calculation. (b) Spin density plot obtained from a Mulliken population analysis (red, positive spin density; yellow, negative spin density).

Table 5, and a qualitative molecular orbital diagram and spin density plot are presented in Figure 11. The BS(1,2) solution slightly overestimates the experimental bond distances. Notably, the C_{imine}−C_{ipso} distances are computed to be 1.423 Å, consistent with a two-electron reduced bis(imino)pyridine ligand[14,20] but longer than the experimental values of 1.400(3) and 1.405(3) Å. This computational solution does, however, successfully reproduce the Mössbauer isomer shift and possibly the quadrupole splitting. Recall that in a zero-field Mössbauer experiment only the absolute value of the quadrupole splitting is measured. This description is also inconsistent with the observed EPR spectrum of $[Na(15\text{-crown-}5)(THF)_2][(^{iPr}PDI)$-

Table 5. Comparison of Experimental and Computed Metrical and Mössbauer Parameters for $[(^{iPr}PDI)Fe(N_2)]^-$ for BS(1,2) and BS(2,1) Solutions; Bond Distances Reported in (Å)

parameter	experimental	BS(1,2)	BS(2,1)
Fe(1)−N(1)	1.8912(18)	1.981	1.937
Fe(1)−N(2)	1.8338(17)	1.891	1.865
Fe(1)−N(3)	1.8858(18)	1.979	1.938
Fe(1)−N(4)	1.784(2)	1.784	1.816
N(3)−C(8)	1.375(3)	1.370	1.386
N(2)−C(7)	1.389(3)	1.368	1.390
N(2)−C(3)	1.391(3)	1.368	1.391
N(1)−C(2)	1.366(3)	1.369	1.385
C(7)−C(8)	1.400(3)	1.423	1.410
C(2)−C(3)	1.405(3)	1.423	1.409
N(4)−N(5)	1.089	1.128	1.121
δ (mm/s)	0.28	0.34	0.35
ΔE_Q (mm/s)	|1.66|	+1.68	−1.71

Fe(N$_2$)] which supports an iron-based SOMO, in contrast to the principally ligand-based radical predicted by the BS(1,2) calculation.

Repeating the DFT calculation using the xyz coordinates from the lower quality crystal structure of [Na(18-crown-6)(THF)$_2$][(^{iPr}PDI)Fe(N$_2$)] produced a different electronic structure description. In this case, a BS(2,1) solution was obtained, +0.37 kcal/mol higher in energy than the BS(1,2) outcome described above. A qualitative molecular orbit diagram and spin density plot for the BS(2,1) solution are presented in Figure 12. This solution was also obtained by a calculation starting from the high-quality structure using a BS(2,1) approach that uses the orbitals of the lowest lying quartet state as the initial guess for the orbitals of the doublet ground state. Such a small energy difference renders the two solutions indistinguishable on the basis of energetic arguments alone. In this case, the computed structure is best described as an intermediate spin ferrous compound with a rare example of a triply reduced bis(imino)pyridine. A three-electron-reduced bis(imino)pyridine with lithium counterions has been previously reported by Gambarotta, Budzelaar and co-workers[38] and more recently by Bart and co-workers in a uranium cyclopentadienyl compound.[39] To the best of our knowledge, a triply reduced bis(imino)pyridine has yet to be identified in transition metal coordination chemistry. In the BS(2,1) solution for $[(^{iPr}PDI)Fe(N_2)]^-$, antiferromagnetic coupling between a d$_{yz}$ orbital on the iron and the singly occupied a$_2$ PDI orbital gives rise to the overall observed doublet ground state. The b$_2$ orbital of the PDI ligand is doubly occupied and accordingly the SOMO of the compound is an iron-centered orbital of principally d$_{z^2}$ parentage. This computed SOMO is consistent with the experimentally observed EPR spectrum that exhibits relatively large g anisotropy, diagnostic of an iron-centered radical. As noted above, the distortion to the bis(imino)pyridine chelate obtained from the X-ray crystal structure of [Na(18-crown-6)][(^{iPr}PDI)Fe(N$_2$)] are also consistent with the published values for [PDI]$^{3-}$.[38] This electronic structure description more accurately reproduces the experimentally observed C$_{imine}$−C$_{ipso}$ distances. The computed values of 1.410 and 1.409 Å are within the acceptable range of the experimental distances of 1.400(3) and 1.405(3) Å, also supporting the BS(2,1) solution as the more accurate description of the electronic structure. In this view, the one
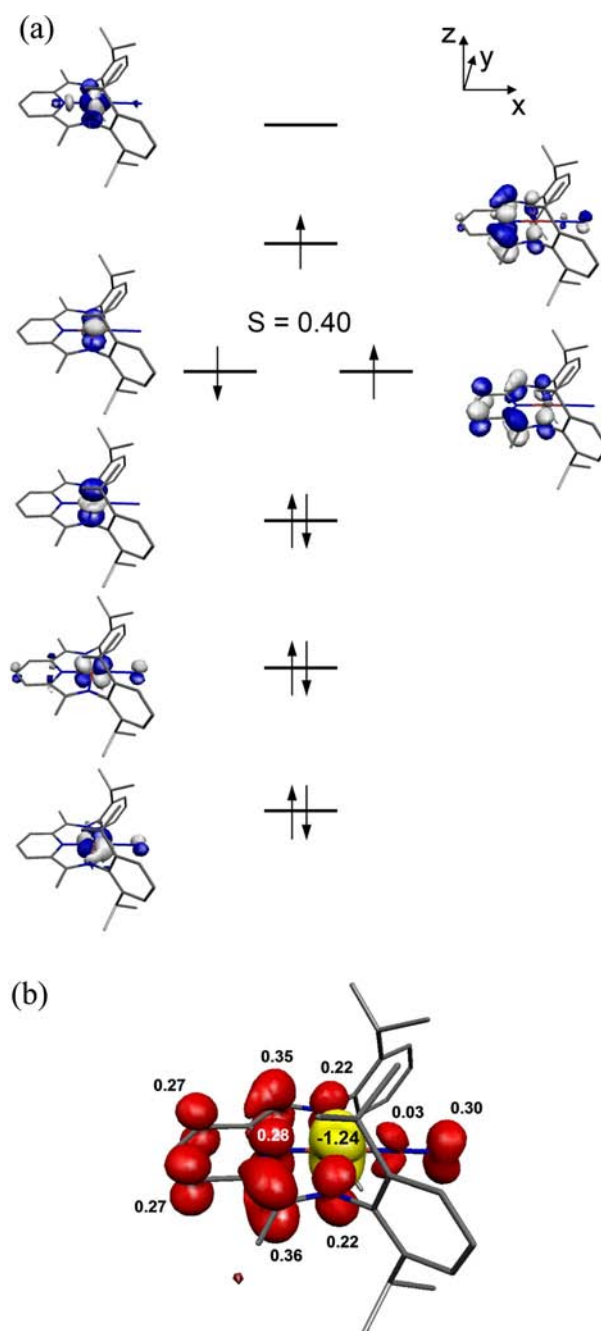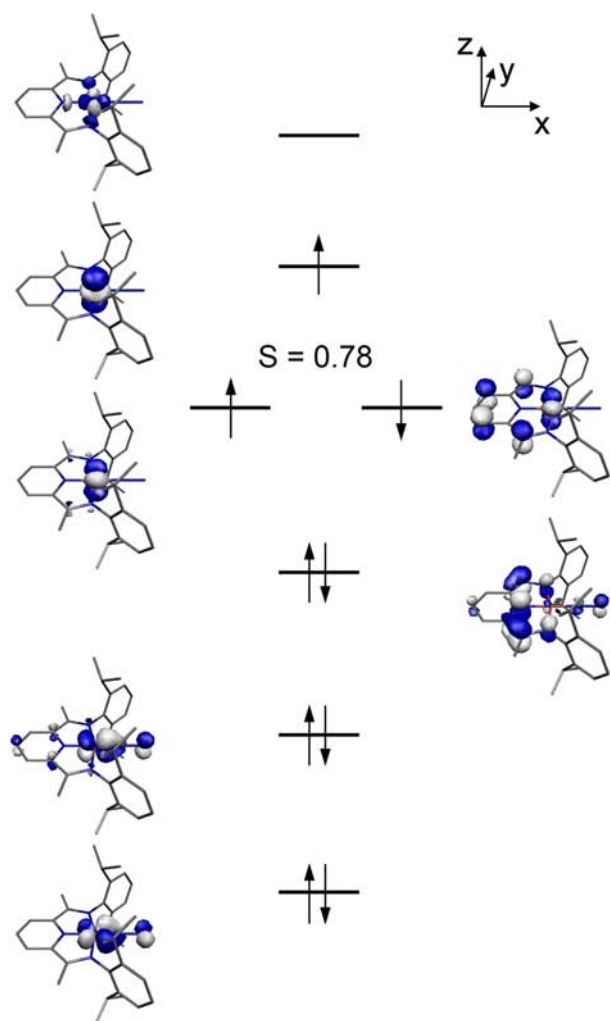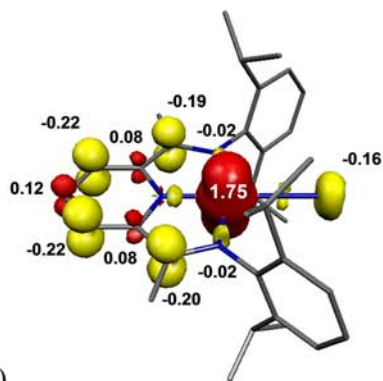

Figure 11. (a) Qualitative molecular orbital diagram for $[(^{iPr}PDI)Fe(N_2)]^-$ from a spin-unrestricted, broken symmetry (1,2) B3LYP DFT calculation. (b) Spin density plot obtained from a Mulliken population analysis (red, positive spin density; yellow, negative spin density).

electron reduction of $[(^{iPr}PDI)Fe(N_2)]$ to $[(^{iPr}PDI)Fe(N_2)]^{1-}$ is principally ligand-based and preserves the intermediate spin ($S_{Fe} = 1$) ferrous center.

The electronic structure of the dianionic bis(imino)pyridine iron dinitrogen complex, $[(^{iPr}BPDI)Fe(N_2)]^{2-}$ was also investigated computationally. The inability to obtain X-ray quality single crystals of the crown ether variant, [Na(18-crown-6)(THF)$_2$]$_2$[(^{iPr}BPDI)Fe(N$_2$)], coupled with the diamagnetism of the compound limits the amount of experimental data available to validate the computational results. As shown from the qualitative molecular orbital diagram and spin density plot presented in Figure 13, a BS(1,1) solution was obtained
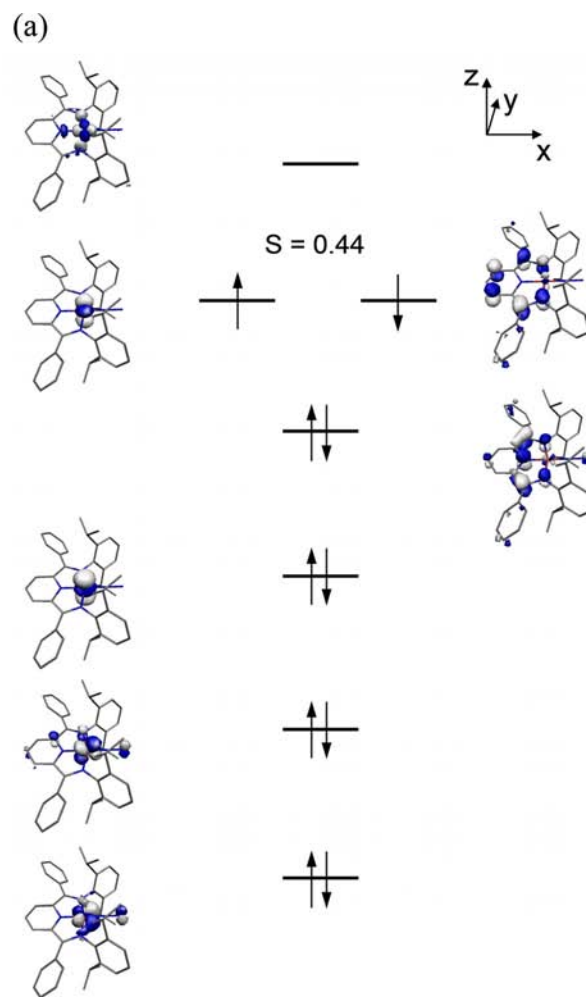
(a)

(b)

Figure 12. (a) Qualitative molecular orbital diagram for $[(^{iPr}PDI)Fe(N_2)]^-$ from a spin-unrestricted, broken symmetry (2,1) B3LYP DFT calculation. (b) Spin density plot obtained from a Mulliken population analysis (red, positive spin density; yellow, negative spin density).

(a)

(b)

Figure 13. (a) Qualitative molecular orbital diagram for $[(^{iPr}BPDI)Fe(N_2)]^{2-}$ from a spin-unrestricted, broken symmetry (1,1) B3LYP DFT calculation. (b) Spin density plot obtained from a Mulliken population analysis (red: positive spin density, yellow: negative spin density).

corresponding to a low-spin Fe(I) compound and a three-electron-reduced bis(imino)pyridine. Thus, the one electron reduction of $[(^{iPr}BPDI^{3-})Fe^{II}(N_2)]^{1-}$ to $[(^{iPr}BPDI^{3-})Fe^I(N_2)]^{2-}$ is metal-based where the intermediate spin ferrous center is reduced to low spin Fe(I).

Electronic Structure Summary. The electronic structures of the series of compounds prepared over four formal oxidation states prepared in this work are summarized in Figure 14. From neutral $(^{iPr}PDI^{2-})Fe^{II}N_2$, both one-electron oxidation and

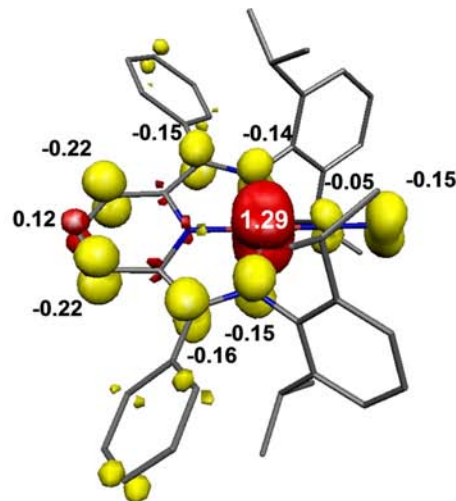reduction are ligand-based as the iron(II) ion is preserved and the redox events occur at the bis(imino)pyridine. The reduction chemistry provided a rare example of a bis(imino)-pyridine trianion. With the appropriate bis(imino)pyridine, two
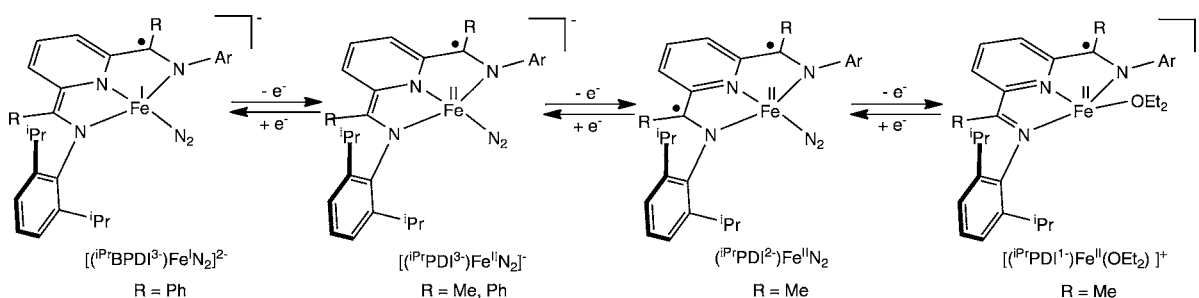
Figure 14. Electronic structure summary of bis(imino)pyridine iron dinitrogen and diethyl ether complexes.

electron reduction of the neutral iron dinitrogen compound is chemically feasible and is the first compound in the series where a metal-based redox event occurs. In considering the entire series, it is noteworthy that three electron transfer events take place before the metal engages in redox chemistry.

Comparing these results to the previously reported bis-(imino)pyridine iron carbonyl series (Figure 2),[23] highlights the impact of both coordination number and identity of the neutral ligand on the overall electronic structure of the compounds. Oxidation of $(^{iPr}PDI)Fe(CO)_2$, a highly covalent molecule best described as hybrid between Fe(0) and Fe(II), yielded $[(^{iPr}PDI^0)Fe^I(CO)_2]^+$, where the bis(imino)pyridine adopts its neutral form. The one-electron event to generate $[(^{iPr}PDI^{2-})Fe^I(CO)_2]^-$ also generates an iron(I) center where the chelate is reduced by two electrons. Substitution of the carbonyl ligands with dinitrogen or diethyl ether results in compounds where the ligand is more reduced. For example, upon oxidation to the diethyl ether cation, $[(^{iPr}PDI^{1-})$-$Fe^{II}(OEt_2)]^+$, the bis(imino)pyridine undergoes a one electron oxidation and maintains radical character. Likewise, reduction of $[(^{iPr}PDI^{2-})Fe^{II}(N)_2]$ to $[(^{iPr}PDI^{3-})Fe^{II}(N_2)]^-$ is solely ligand based and highlights that in the absence of other π-acid ligands, the bis(imino)pyridine mitigates the redox chemistry in the complex.

■ EXPERIMENTAL SECTION

General Considerations. All air- and moisture-sensitive manipulations were carried out using standard vacuum line, Schlenk, and cannula techniques or in an MBraun inert atmosphere drybox containing an atmosphere of purified nitrogen. Solvents for air- and moisture-sensitive manipulations were initially dried and deoxygenated using literature procedures.[40] Benzene-d_6 was purchased from Cambridge Isotope Laboratories and dried over 4 Å molecular sieves.

^1H NMR spectra were recorded on Varian Mercury 300, Inova 400, 500, and 600 spectrometers operating at 299.76, 399.78, 500.62, and 599.78 MHz, respectively. ^{13}C NMR spectra were recorded on an Inova 500 spectrometer operating at 125.893 MHz. All ^1H and ^{13}C NMR chemical shifts are reported relative to SiMe$_4$ using the ^1H (residual) and ^{13}C chemical shifts of the solvent as a secondary standard. Peak widths at half heights are reported for paramagnetically broadened and shifted resonances. Solution magnetic moments were determined by Evans method using a ferrocene standard and are the average value of at least two independent measurements. Gouy balance measurements were performed with a Johnson Matthey instrument that was calibrated with HgCo(SCN)$_4$. Infrared spectra were collected on a Thermo Nicolet spectrometer. Elemental analyses were performed at Robertson Microlit Laboratories, Inc., in Ledgewood, NJ. SQUID magnetization data of crystalline powdered samples were recorded with a SQUID magnetometer (Quantum Design) at 10 kOe between 5 and 300 K for all samples. Values of the magnetic susceptibility were corrected for the underlying diamagnetic increment using tabulated Pascal constants and the effect of the blank sample holders (gelatin capsule/straw). The program julX, written by E. Bill,

was used for (elements of) the simulation and analysis of magnetic susceptibility.[41]

Single crystals suitable for X-ray diffraction were coated with polyisobutylene oil in a drybox, transferred to a nylon loop and then quickly transferred to the goniometer head of a Bruker X8 APEX2 diffractometer equipped with a molybdenum X-ray tube (λ = 0.71073 Å). Preliminary data revealed the crystal system. A hemisphere routine was used for data collection and determination of lattice constants. The space group was identified and the data were processed using the Bruker SAINT+ program and corrected for absorption using SADABS. The structures were solved using direct methods (SHELXS) completed by subsequent Fourier synthesis and refined by full-matrix least-squares procedures.

X-band EPR derivative spectra were recorded on a Bruker ELEXSYS E500 spectrometer equipped with the Bruker standard cavity (ER4102ST) and a helium flow cryostat (Oxford Instruments ESR 910). Microwave frequencies were calibrated with a Hewlett-Packard frequency counter (HP5353B), and the field control was calibrated with a Bruker NMR field probe (ER035M). The spectra were simulated with the program GFIT by Eckhard Bill for the calculation of powder spectra with effective g values and anisotropic line widths (Lorentzian line shapes were used).

Zero field ^{57}Fe Mössbauer spectra were collected on a SEE Co. Mössbauer spectrometer (MS4) with a $^{57}Co/Rh$ radiation source, at 80 K in constant acceleration mode. The temperature in the sample chamber was controlled by a Janis Research Co. CCS-850 He/N$_2$ cryostat within an accuracy of ±0.3 K. The data were calibrated relative to an α-iron at 298, with minimum experimental line widths of 0.23 mm/s. The fitting procedure to extract quantitative spectral parameters uses a least-squares Lorentzian fitting method using the WMOSS software developed by SEE Co.

Quantum-chemical calculations. All DFT calculations were performed with the ORCA program package[42] as described previously.[21,23] The geometry optimizations of the complexes and single-point calculations on the optimized geometries were carried out at the B3LYP level of DFT. This hybrid functional often gives better results for transition metal compounds than pure gradient-corrected functionals, especially with regard to metal–ligand covalency. Throughout this paper we describe our computational results by using the broken-symmetry (BS) approach by Ginsberg and Noodleman.[35,36] Because several broken symmetry solutions to the spin-unrestricted Kohn−Sham equations may be obtained, the general notation BS(m,n) has been adopted, where m (n) denotes the number of spin-up (spin-down) electrons at the two interacting fragments.[36] Canonical and corresponding orbitals, as well as spin density plots were generated with the program Molekel.

Preparation of $[(^{iPr}PDI)Fe(OEt_2)][BAr^F_4]$. A 20 mL scintillation vial was charged with 0.140 g (0.236 mmol) of $(^{iPr}PDI)Fe(N_2)_2$, 0.247 g (0.236 mmol) of $[Cp_2Fe][BAr^F_4]$ and a stir bar. Approximately 7 mL of diethyl ether were added to the mixture of solids with stirring. The reaction evolved nitrogen gas immediately and changed color from light to dark green. After gas evolution ceased, pentane was added and the scintillation vial was stored at −35 °C. Over time a light green solid precipitated. The solid was collected on a glass frit and washed with 4 x ~ 20 mL of pentane. The solid was dried in vacuo and yielded 0.250 g (73%) of a light green powder identified as $[(^{iPr}PDI)Fe-$

(OEt$_2$)][BAr$^F_4$]. Single crystals were obtained from a fluorobenzene-pentane mixture stored at −35 °C. Anal, for C$_{69}$H$_{65}$N$_3$FeBF$_{24}$O: Calcd C, 56.19; H, 4.44; N, 2.85. Found: C, 56.34; H, 4.67; N, 2.81. Solid-state magnetic susceptibility (23 °C): μ_{eff} = 5.2 μ_B. ^{1}H NMR (benzene-d_6): δ = 1.29 (569 Hz, Et$_2$O), 4.12 (370 Hz, Et$_2$O), 8.44 (18 Hz), 9.67 (12 Hz). ^{19}F NMR (benzene-d_6): δ = 62.30.

Preparation of [Na(THF)$_n$][(^{iPr}PDI)Fe(N$_2$)]. A scintillation vial was charged with 0.004 g (0.174 mmol) of sodium and 0.022 g (0.182 mmol) of naphthalene followed by approximately 5 mL of THF. The solution was stirred until the sodium was completely dissolved. Once this occurred, a solution containing 0.100 g (0.168 mmol) of (^{iPr}PDI)Fe(N$_2$)$_2$ in THF was added. The resulting reaction mixture was filtered through Celite and the volatiles were removed in vacuo. The residue was washed with diethyl ether and the solid was collected on a glass frit and washed with pentane and dried under vacuum, yielding 0.090 g of a product identified as [Na(THF)$_n$][(^{iPr}PDI)Fe(N$_2$)]. IR (KBr): ν(N$_2$) = 1966, 1914 cm^{-1}.

Preparation of [Na(15-crown-5)(THF)$_2$][(^{iPr}PDI)Fe(N$_2$)]. A scintillation vial was charged with 0.006 g (0.261 mmol) of sodium, 0.037 g (0.287 mmol) of naphthalene and approximately 10 mL of THF. The solution was stirred until the sodium was completely dissolved. Once this occurred, the sodium naphthalenide solution was added dropwise to a solution containing 0.155 g (0.261 mmol) of (^{iPr}PDI)Fe(N$_2$)$_2$ in THF. The resulting reaction mixture was filtered through Celite and 0.060 g (0.274 mmol) of 15-crown-5 was added and the volatiles were removed. The residue was dissolved in minimal THF and crystallized at −35 °C, yielding yielding 0.104 g (42%) of a product identified as [Na(15-crown-5)(THF)$_2$][(^{iPr}PDI)Fe(N$_2$)]. Single crystals were obtained from a THF-pentane mixture stored at −35 °C. Anal. Calcd for C$_{51}$H$_{79}$FeN$_5$NaO$_7$: C, 64.27; H, 8.36; N, 7.35. Found: C, 63.99; H, 8.01; N, 7.04. Solid-state magnetic susceptibility (23 °C): μ_{eff} = 1.9 μ_B. IR (KBr): ν(N$_2$) = 1956 cm^{-1}.

Preparation of [Na(18-crown-6)(THF)$_2$][(^{iPr}PDI)Fe(N$_2$)]. A scintillation vial was charged with 0.012 g (0.522 mmol) of sodium, 0.075 g (0.575 mmol) of naphthalene, and approximately 10 mL of THF. The solution was stirred until the sodium was completely dissolved. Once this occurred, the sodium naphthalenide solution was added dropwise to a solution containing 0.310 g (0.522 mmol) of (^{iPr}PDI)Fe(N$_2$)$_2$ in THF. The resulting reaction mixture was filtered through Celite and 0.140 g (0.530 mmol) of 18-crown-6 was added and the volatiles were removed. The residue was dissolved in THF and the product was precipitated with excess pentane. The resulting dark brown powder was collected on a glass frit and washed with pentane and dried under vacuum, yielding 0.390 g (75%) of a product identified as [Na(18-crown-6)(THF)$_2$][(^{iPr}PDI)Fe(N$_2$)]. Single crystals were obtained from a THF-pentane mixture stored at −35 °C. Anal. Calcd for C$_{53}$H$_{81}$FeN$_5$NaO$_8$: C, 63.84; H, 8.39; N, 7.02. Found: C, 63.77; H, 7.94; N, 6.71. Solid-state magnetic susceptibility (23 °C): μ_{eff} = 1.8 μ_B. IR (KBr): ν(N$_2$) = 1949 cm^{-1}.

Preparation of [Na(THF)$_n$][(^{iPr}BPDI)Fe(N$_2$)]. This molecule was prepared in a similar manner to [Na(THF)$_n$][(^{iPr}PDI)Fe(N$_2$)] with 0.004 g (0.174 mmol) of sodium, 0.022 g (0.182 mmol) of naphthalene, and a THF solution containing 0.120 g (0.168 mmol) of (^{iPr}BPDI)Fe(N$_2$)$_2$. This procedure furnished 0.083 g of a pink powder identified as [Na(THF)$_n$][(^{iPr}BPDI)Fe(N$_2$)]. IR (KBr): ν(N$_2$) = 1979, 1932 cm^{-1}.

Preparation of [Na(18-crown-6)(THF)$_2$][(^{iPr}BPDI)Fe(N$_2$)]. This molecule was prepared in a similar manner to [Na(18-crown-6)(THF)$_2$][(^{iPr}PDI)Fe(N$_2$)] with 0.012 g (0.522 mmol) of sodium, 0.075 g (0.575 mmol) of naphthalene, 0.140 g (0.174 mmol) of (^{iPr}BPDI)FeBr$_2$ and 0.050 g (0.190 mmol) of 18-crown-6. This procedure yielded 0.139 g (73%) of a bright pink powder identified as [Na(18-crown-6)(THF)$_2$][(^{iPr}PDI)Fe(N$_2$)]. Anal. Calcd for C$_{63}$H$_{87}$FeN$_5$NaO$_8$: C, 67.49; H, 7.82; N, 6.25. Found: C, 67.55; H, 7.80; N, 6.21. Solid-state magnetic susceptibility (23 °C): μ_{eff} = 1.7 μ_B. IR (KBr): ν(N$_2$) = 1971 cm^{-1}.

Synthesis of [Na(THF)$_n$]$_2$[(^{iPr}BPDI)Fe(N$_2$)]. A scintillation vial was charged with 0.008 g (0.348 mmol) of sodium, 0.045 g (0.364 mmol) of naphthalene and approximately 5 mL of THF. This solution was stirred until the sodium was dissolved completely and then a solution

of 0.120 g of (^{iPr}BPDI)Fe(N$_2$)$_2$ in THF was added with stirring. The resulting reaction mixture was filtered through Celite and the volatiles were reduced in vacuo. The residue was extracted into diethyl ether, filtered through Celite and the volume reduced by to approximately half. An equal volume of pentane was added and the solution was cooled to −35 °C. The solid was collected on a glass frit and washed with pentane and dried under vacuum and furnished 0.110 g of a product identified as [Na(THF)$_n$]$_2$[(^{iPr}BPDI)Fe(N$_2$)]. IR (KBr): ν(N$_2$) = 1908, 1830 cm^{-1}.

Preparation of [Na(18-crown-6)(THF)$_2$]$_2$[(^{iPr}BPDI)Fe(N$_2$)]. A scintillation vial was charged with 0.020 g (0.869 mmol) of sodium and 0.125 g (0.958 mmol) of naphthalene followed by approximately 10 mL of THF. The solution was stirred until the sodium was completely dissolved. Once this occurred, the sodium naphthalenide solution was added dropwise to a solution containing 0.175 g (0.216 mmol) of (^{iPr}BPDI)FeBr$_2$ in THF. The resulting reaction mixture was filtered through Celite and 0.115 g (0.435 mmol) of 18-crown-6 was added and the volatiles were removed. The residue was dissolved in THF and the product was precipitated with excess pentane and the dark purple powder was collected on a glass frit and washed with pentane and dried under vacuum, yielding 0.235 g (70%) of a product identified as [Na(18-crown-6)(THF)$_2$]$_2$[(^{iPr}BPDI)Fe(N$_2$)]. Single crystals were obtained from a concentrated diethyl ether solution stored at −35 °C. Anal. Calcd for C$_{83}$H$_{127}$FeN$_5$Na$_2$O$_{16}$: C, 64.20; H, 8.24; N, 4.51. Found: C, 63.96; H, 8.08; N, 3.92. IR (KBr): ν(N$_2$) = 1887 cm^{-1}.

ASSOCIATED CONTENT

Ⓢ Supporting Information

Crystallographic details for [(^{iPr}PDI)Fe(OEt$_2$)][BAr$^F_4$], [Na-(15-crown-5)(THF)$_2$][(^{iPr}PDI)Fe(N$_2$)], [Na(18-crown-6)-(THF)$_2$][(^{iPr}PDI)Fe(N$_2$)], and [Na(THF)$_2$][Na(OEt$_2$)$_2$]-[(^{iPr}BPDI)Fe(N$_2$)] in CIF format. This material is available free of charge via the Internet at http://pubs.acs.org.

AUTHOR INFORMATION

Corresponding Author
*E-mail: pchirik@princeton.edu.

Notes
The authors declare no competing financial interest.

ACKNOWLEDGMENTS

REFERENCES

(1) Hazari, N. *Chem. Soc. Rev.* **2010**, *39*, 4044.
(2) Rodriguez, M. M.; Bill, E.; Brennessel, W. W.; Holland, P. L. *Science* **2011**, *334*, 780.
(3) Bart, S. C.; Lobkovsky, E.; Chirik, P. J. *J. Am. Chem. Soc.* **2004**, *126*, 13794.
(4) Archer, A. M.; Bouwkamp, M. W.; Cortez, M.-P.; Lobkovsky, E.; Chirik, P. J. *Organometallics* **2006**, *25*, 4269.
(5) Trovitch, R. J.; Lobkovsky, E.; Bill, E.; Chirik, P. J. *Organometallics* **2008**, *27*, 1470.
(6) Russell, S. K.; Darmon, J. M.; Lobkovsky, E.; Chirik, P. J. *Inorg. Chem.* **2010**, *49*, 2782.
(7) Tondreau, A. M.; Atienza, C. C. H.; Weller, K. J.; Nye, S. A.; Lewis, K. M.; Delis, J. G. P.; Chirik, P. J. *Science* **2012**, *335*, 567.

(8) Tondreau, A. M.; Lobkovsky, E.; Chirik, P. J. *Org. Lett.* **2008**, *10*, 2789.

(9) Bouwkamp, M. W.; Bowman, A. C.; Lobkovsky, E.; Chirik, P. J. *J. Am. Chem. Soc.* **2006**, *128*, 13340.

(10) Russell, S. K.; Lobkovsky, E.; Chirik, P. J. *J. Am. Chem. Soc.* **2011**, *133*, 8858.

(11) Sylvester, K. T.; Chirik, P. J. *J. Am. Chem. Soc.* **2009**, *131*, 8772.

(12) Gibson, V. C.; Redshaw, C.; Solan, G. A. *Chem. Rev.* **2007**, *107*, 1745.

(13) Chirik, P. J. *Inorg. Chem.* **2011**, *50*, 9737.

(14) Knijnenburg, Q.; Gambarotta, S.; Budzelaar, P. H. M. *Dalton Trans.* **2006**, 5442.

(15) Kuwabara, I. H.; Comninos, F. C. M.; Pardini, V. L.; Viertler, H.; Toma, H. E. *Electrochim. Acta* **1994**, *39*, 2401.

(16) Toma, H. E.; Chavez-Gil, T. E. *Inorg. Chim. Acta* **1997**, *257*, 197.

(17) de Bruin, B.; Bill, E.; Bothe, E.; Weyhermüller, T.; Wieghardt, K. *Inorg. Chem.* **2000**, *39*, 2936.

(18) Budzelaar, P. H. M.; de Bruin, B.; Gal, A. W.; Wieghardt, K.; van Lenthe, J. H. *Inorg. Chem.* **2001**, *40*, 4649.

(19) Blanchard, S.; Derat, E.; Desage-El Murr, M.; Fensterbank, L.; Malacria, M.; Mouriès-Mansuy, V. *Eur. J. Inorg. Chem.* **2012**, 376.

(20) Bart, S. C.; Chlopek, K.; Bill, E.; Bouwkamp, M. W.; Lobkovsky, E.; Neese, F.; Wieghardt, K.; Chirik, P. J. *J. Am. Chem. Soc.* **2006**, *128*, 13901.

(21) Stieber, S. C. E.; Milsmann, C.; Hoyt, J. M.; Turner, Z. R.; Finkelstein, K. D.; Wieghardt, K.; DeBeer, S.; Chirik, P. J. *Inorg. Chem.* **2012**, *51*, 3770.

(22) Bart, S. C.; Lobkovsky, E.; Bill, E.; Wieghardt, K.; Chirik, P. J. *Inorg. Chem.* **2007**, *46*, 7055.

(23) Tondreau, A. M.; Milsmann, C.; Lobkovsky, E.; Chirik, P. J. *Inorg. Chem.* **2011**, *50*, 9888.

(24) (a) Knijnenburg, D.; Hetterscheid, D.; Kooistra, T. M.; Budzelaar, P. H. M. *Eur. J. Inorg. Chem.* **2004**, 1204. (b) Zhu, D.; Thapa, I.; Korobkov, I.; Gambarotta, S.; Budzelaar, P. H. M. *Inorg. Chem.* **2011**, *50*, 9879.

(25) Bowman, A. C.; Bart, S. C.; Heinemann, F. W.; Meyer, K.; Chirik, P. J. *Inorg. Chem.* **2009**, *48*, 5587.

(26) Scott, J.; Vidyaratne, I.; Korobkov, I.; Gambarotta, S.; Budzelaar, P. H. M. *Inorg. Chem.* **2008**, *47*, 896.

(27) Bowman, A. C.; Milsmann, C.; Atienza, C. C. H.; Lobkovsky, E.; Wieghardt, K.; Chirik, P. J. *J. Am. Chem. Soc.* **2010**, *132*, 1676.

(28) Lee, Y.; Mankad, N. P.; Peters, J. C. *Nat. Chem* **2010**, *2*, 558.

(29) Atienza, C. C. H.; Milsmann, C.; Lobkovsky, E.; Chirik, P. J. *Angew. Chem., Int. Ed.* **2011**, *50*, 8143.

(30) Scott, J.; Gambarotta, S.; Korobkov, I.; Budzelaar, P. H. M. *J. Am. Chem. Soc.* **2005**, *127*, 13019.

(31) Bouwkamp, M. W.; Lobkovsky, E.; Chirik, P. J. *Inorg. Chem.* **2006**, *45*, 2.

(32) Sugiyama, H.; Aharonian, G.; Gambarotta, S.; Yap, G. P. A.; Budzelaar, P. H. M. *J. Am. Chem. Soc.* **2002**, *124*, 12268.

(33) Vidyaratne, I.; Scott, J.; Gambarotta, S.; Budzelaar, P. H. M. *Inorg. Chem.* **2007**, *46*, 7040.

(34) Darmon, J. M.; Turner, Z. R.; Lobkovsky, E.; Chirik, P. J. *Organometallics* **2012**, *31*, 2275.

(35) Ginsberg, A. P. *J. Am. Chem. Soc.* **1980**, *102*, 111.

(36) Noodleman, L.; Peng, C. Y.; Case, D. A.; Mouesca, J. M. *Coord. Chem. Rev.* **1995**, *144*, 199.

(37) Kirchner, B.; Wennmohs, F.; Ye, S.; Neese, F. *Curr. Opin. Chem. Biol.* **2007**, *11*, 134.

(38) Enright, D.; Gambarotta, S.; Yap, G. P. A.; Budzelaar, P. H. M. *Angew. Chem., Int. Ed.* **2002**, *41*, 3873.

(39) Cladis, D. C.; Kiernicki, J. J.; Fanwick, P. E.; Bart, S. C. *Chem. Commun.*, DOI:10.1039/C2CC37193F.

(40) Pangborn, A. B.; Giardello, M. A.; Grubbs, R. H.; Rosen, R. K.; Timmers, F. J. *Organometallics* **1996**, *15*, 1518.

(41) http://ewww.mpi-muelheim.mpg.de/bac/logins/bill/julX_en.php.

(42) Neese, F. *Orca - an ab initio, DFT and Semiempirical Electronic Structure Package*, Version 2.8, Revision 2287; Institut für Physikalische und Theoretische Chemie, Universität Bonn: Bonn, Germany, November 2010.

646

dx.doi.org/10.1021/ic301675t | *Inorg. Chem.* 2013, 52, 635−646